

Performance of DØ detector in Run II

D. Buchholz, for the DØ Collaboration

Northwestern University, Evanston, IL USA

Received: 15 October 2003 / Accepted: 10 March 2004 /
Published Online: 31 March 2004 – © Springer-Verlag / Società Italiana di Fisica 2004

Abstract. The DØ experiment, upgraded for Run II, has resumed data taking with a much improved detector. The upgrade components and their performance are described.

PACS. 29.40.Gx Tracking and position-sensitive detectors – 29.40.Vj Calorimeters

1 Introduction

The Fermilab accelerator has undergone a series of upgrades to increase the beam energy and intensity. The accelerator started in spring 2001 with its turn on and commissioning of the new main ring accelerator and tevatron complex. To take advantages of these improvements the DØ experiment upgraded most of its components; calorimeter, muon tracking, triggering, tracking, and associated electronics. Preliminary physics results are being presented at this conference in other sessions [1].

2 Fermilab accelerator upgrades

To increase the \bar{p} yield and luminosity, a new main ring was constructed as an injector to the Tevatron and improvements were made to the booster and \bar{p} source. The center of mass energy of the collider was increased from 1.8 TeV for Run I to 1.98 TeV for Run II. An increase of 9% in beam energy raises the cross section of top production by 30% to 40%. To reduce the number of interactions per bunch crossing, the number of bunches in each beam was increased from 6 to 36. This reduced the time between crossing from 3500 ns to 396 ns. Run I achieved a total integrated luminosity of 0.14 fb^{-1} . The goal of Run II is to achieve between 4.0 fb^{-1} and 8.0 fb^{-1} .

3 DØ detector

The components of the DØ detector that remained the same from Run I to the current run, include the liquid Argon-Uranium calorimeter, the central muon tracker, and the muon toroid. New for the current run are a magnetic tracker, preshower detectors, forward muon detectors, and forward proton detectors. Substantial improvements were made to the front end electronics, the data acquisition system, and the trigger systems.

The implementation of the magnetic tracker was completed in April 2002. Since that time, DØ has received 0.23 fb^{-1} in integrated luminosity, and the DØ experiment has steadily improved its efficiency for data collection. The live time of the experiment was about 40% over a year ago and is now almost at 90%. DØ has collected data from 0.17 fb^{-1} in luminosity from April of last year to mid-July 2003.

4 Magnetic tracker

For Run II the drift chamber tracker of Run I was removed and replaced with a magnetic tracker consisting of a 2T superconducting solenoid magnet with a silicon microstrip and scintillating fiber tracker within the magnet volume [2].

4.1 Silicon microstrip tracker

The Silicon Microstrip Tracker (SMT) consists of 6 barrels with 4 layers arranged axially around the beam pipe and interspersed with 16 radial disks. This design optimized the tracking and vertexing capability over $|\eta| < 3$. The beam interaction length is $\sigma \simeq 25cm$. The components of this detector are listed in Table 1. The silicon microstrip sensors are constructed out of either single sided or double sided technology depending on where they are being used. The pitch of the silicon strips varies from 50 μm to 80 μm again depending on the component. The readout of the microstrips is accomplished using a custom chip, SVX2, developed jointly by LBL and FNAL [3] to read out and digitize 128 channels each. The silicon tracker is mechanically supported by a beryllium structure to minimize material near the beam and cooled to $-10^{\circ}C$ in normal operation.

Table 1. Components of Silicon Microstrip Tracker

	Barrels	F-disks	H-disks
Type	double + single	double sided	single sided
Stereo Angle	$0^{\circ}, 2^{\circ}, 90^{\circ}$	$\pm 15^{\circ}$	$\pm 7.5^{\circ}$
Channels	$\sim 400K$	$\sim 250K$	$\sim 150K$
Inner Radius	2.7cm	2.6cm	9.5cm
Outer Radius	9.4cm	10.5cm	26cm

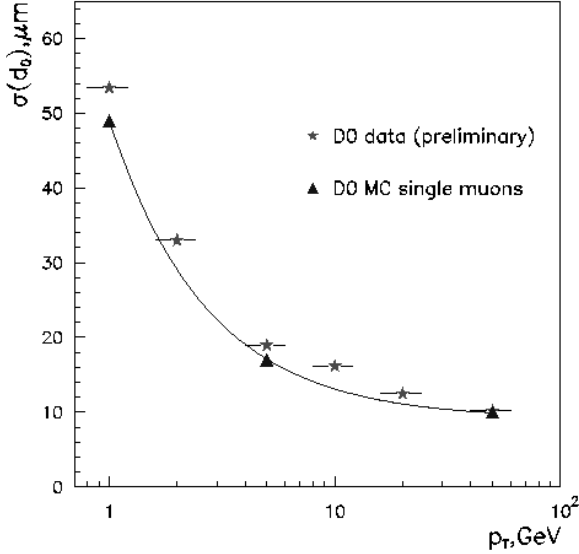


Fig. 1. Impact parameter resolution for single μ 's projected back to the interaction point as a function of the p_T of the μ . The Monte Carlo simulation is shown as a *smooth curve* which is somewhat better than the data

4.2 Central fiber tracker

The Central Fiber Tracker (CFT) consists of 8 layers each with a doublet of scintillating fibers positioned axially around the SMT. These are arranged in a barrel geometry similar to the SMT. The scintillation light signals are brought out using fiber optics to a VLPC. The VLPC is a high efficiency solid state photon counter operated at $90^{\circ}K$. These devices have a quantum efficiency approaching 85%. Their signal to noise ratio is excellent and clearly shows the difference between 1, 2, 3, etc. photo-electrons [4].

Vertexing performance is shown in Fig. 1 which plots the distance of closest approach to the interaction point for single muon tracks as a function of p_T of the μ . The data is approaching the solid curve which is the Monte Carlo prediction for the distance of closest approach. The experimental value is $53 \mu m$ at a $p_T = 1 \text{ GeV}$ and improves with higher p_T .

5 Calorimetry

The liquid Argon-Uranium plate sampling calorimeter from Run I is being reused for the current Run II. This

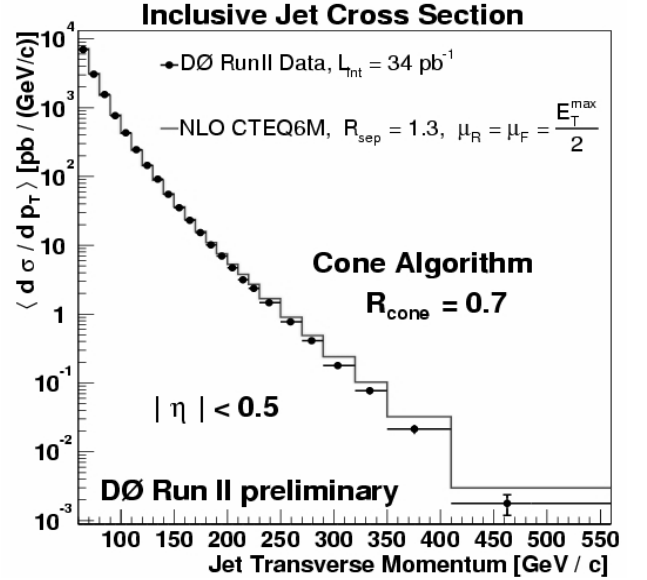


Fig. 2. Inclusive jet cross section as a function of the jet transverse momentum. The *histogram* was obtained from Monte Carlo using the CTEQ6M parameterization of PDF's. The jet energy scale uncertainty is not shown in this figure. When it is folded in, there is no statistically significant deviation from the data

detector has been described in detail previously [5]. The resolution has been measured in a test beam to be $\sigma_E/E = 15\%/\sqrt{E} \oplus 0.3\%$ for electrons and $\sigma_E/E = 45\%/\sqrt{E} \oplus 4\%$ for charged pions. Additional sampling of energy before the calorimeter is provided by scintillating material between the solenoid and central calorimeter (Central Preshower, CPS), in front of the forward calorimeter (Forward Preshower, FPS) and between the central and forward cryostat (Intercryostat Detector, ICD). The preshower detectors are constructed with three layers of scintillating fibers read out with VLPC's, as for the CFT described above.

The ability of the calorimeter to reconstruct energy deposition over seven orders of magnitude in cross section is shown in Fig. 2. This compares the measured differential cross section per p_T with a Monte Carlo calculation based on the CTEQ6M parameterization of PDF's. When the jet energy scale uncertainty is folded into this preliminary result, there are no statistically significant deviations from this NLO QCD calculation.

6 Muon detectors

The muon detector in the central region ($|\eta| < 1$) consists of three layers of drift tubes and scintillators with a toroidal magnet between the first and second layer. This system was used during Run I. The Run I forward muon system ($1 < \eta < 2$) was replaced with 3 layers of mini drift tubes and pixel scintillator counters arranged with a toroidal magnet between the first and second layers also.

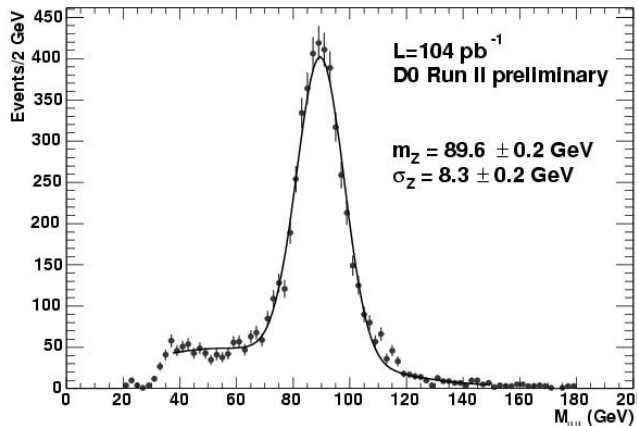


Fig. 3. Invariant dimuon mass in the $Z \rightarrow \mu^+ \mu^-$ region

Additional shielding was placed around the beam pipe to reduce backgrounds before Run II began. The readout and trigger electronics for these systems was completely replaced for the current run.

Dimuon events are reconstructed to form an invariant mass. Based on about 70% of the collected luminosity, the $J/\Psi \rightarrow \mu^+ \mu^-$ signal has more than 150,000 events. The reconstructed mass is $3.071 \pm 0.076 \text{ GeV}/c^2$. The ψ' is reconstructed at $3.670 \pm 0.070 \text{ GeV}/c^2$ based on $\sim 4,100$ events. Both these masses are consistent with that of the Particle Data Group (PDG) world average [6]. Figure 3 shows the reconstructed invariant mass of dimuon events in the vicinity of the Z mass. The preliminary values shown in the figure are consistent with the PDG world average.

7 Triggers and data acquisition

The Fermilab beam operates with a 396 ns crossing time between interactions. DØ employs three levels of trigger computers to reduce this maximum possible interaction rate to 50 Hz which can be written to magnetic media. The output rate from the first level is currently reduced to 1.4 kHz and uses analog information from the calorimeter along with preliminary tracking information from the muon and CFT detectors. The second level of trigger computers use more refined tracking information from the muon and CFT detectors to further reduce the output rate to 800 Hz. The third level of triggering has access to all the data from each event and further selects potentially interesting events which reduces the output rate to 50 Hz which is written directly to disk. Upgrades and further refinements are underway that will allow the first two trigger level to sustain higher input rates and to allow more selectivity based on tracking and vertex information from the SMT and CFT.

The ability of the trigger system to handle the dijet trigger rate is shown in Fig. 4. The raw trigger rate covers

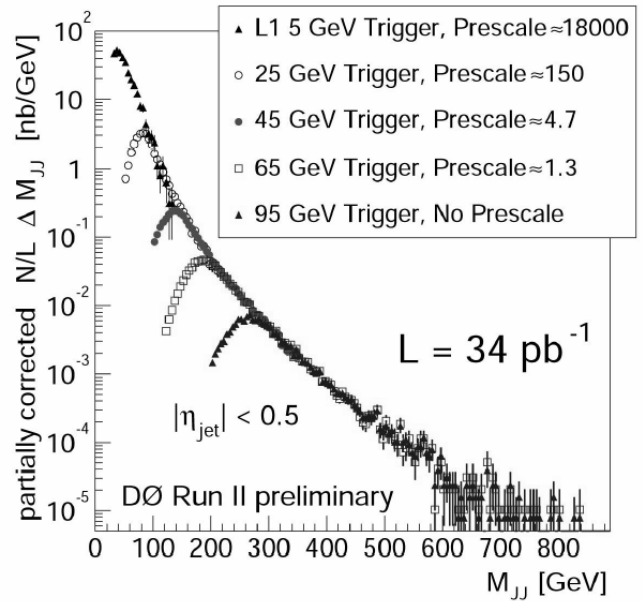


Fig. 4. Dijet mass trigger selection

7 orders of magnitude over the range in mass of the dijet pair. This range is covered by 5 separate triggers each with its own prescale factor and threshold value. After correcting for the prescale factor, the data overlaps cleanly from one region to the next.

8 Summary

There are many preliminary physics results from Run II presented at this conference. The Fermilab luminosity has not increased as quickly as expected, nonetheless we now have almost twice as much data on tape as we had from the entire Run I data. The data collection efficiency has dramatically improved and DØ is now taking high quality data with close to 90% efficiency. Results presented here include SUSY, Higgs, and other new phenomena limits, heavy quarks (b and t), QCD, and electroweak results [1].

References

1. See other DØ contributions in these proceedings
2. S. Abachi, et al.: in preparation for submission to Nucl. Instrum. Methods Phys. Res. A
3. T. Zimmerman, et al.: IEEE Trans. Nucl. Sci. **NS-42**, 803 (1995)
4. A. Bross, et al.: Nucl. Instrum. Methods Phys. Res. A **477**, 172 (2002)
5. S. Abachi, et al.: Nucl. Instrum. Methods Phys. Res. A **338**, 185 (1994)
6. K. Hagiwara, et al.: Phys. Rev. D **66**, 010001 (2002)